Polyhedron 135 (2017) 189–194

Contents lists available at ScienceDirect

Polyhedron

journal homepage: www.elsevier.com/locate/poly

Influence of the charge of the complex unit on the SCO properties in pyrazolyl-pyridinyl-benzimidazole based Fe(II) complexes

C. Rajnák [a,b,c,*], B. Schäfer [b], I. Šalitroš [d], O. Fuhr [b,e], M. Ruben [b,c,*], R. Boča [a,*]

[a] Department of Chemistry, Faculty of Natural Sciences, University of SS Cyril and Methodius, 91701 Trnava, Slovakia
[b] Institute of Nanotechnology, Karlsruhe Institute of Technology (KIT), 76021 Karlsruhe, Germany
[c] IPCMS-CNRS, Université de Strasbourg, 23, rue du Loess, f-67034 Strasbourg, France
[d] Institute of Inorganic Chemistry, FCHPT, Slovak University of Technology, SK-812 37 Bratislava, Slovakia
[e] Karlsruhe Nano-Micro Facility (KNMF), Karlsruhe Institute of Technology (KIT), 76021 Karlsruhe, Germany

ARTICLE INFO

Article history:
Received 6 April 2017
Accepted 24 June 2017
Available online 1 July 2017

Keywords:
Fe(II) complex
Crystal structure
Spin crossover
LIESST effect
Magnetic measurements

ABSTRACT

A tridentate ligand 2-(6-pyrazol-1-yl-pyridin-2-yl)-1H-benzimidazole (**L_1H**) has been synthesized and characterized by NMR, UV–Vis, IR and MS spectroscopy. Starting from **L_1H**, two complexes have been prepared, one containing a complex dication counterbalanced by anions, $[Fe(\mathbf{L_1H})_2](BF_4)_2$ (**1**), and the other one is a charge neutral complex $[Fe(\mathbf{L_1})_2]$ (**2**). The distorted octahedral coordination of **1** was confirmed by X-ray diffraction analysis. Both complexes show a thermally induced spin crossover with the critical temperature lying above the room temperature. The photomagnetic investigation confirmed the LIESST effect for both compounds.

1. Introduction

Fe(II) complexes are known as systems with interesting magnetic properties. In particular, those which show changes between low spin (LS) diamagnetic and high spin (HS) paramagnetic states in d orbitals after physical influences [1]. Spin crossover (SCO) phenomenon among Fe(II) complexes is well documented by a plethora of examples [2–8]. However, still most exciting are the systems with transition temperature close to the room temperature [9] and eventually accompanied by a broad thermal hysteresis. Also volatile charge-neutral complexes are interesting due to their capability of deposition onto surfaces [10,11]. Therefore, logical steps lead to synthesis and common study of ionic and charge-neutral Fe(II) complexes.

The transition temperature is controlled by the balance between the enthalpy and the entropy of the spin transition (both positive), since $T_c = \Delta H/\Delta S$ holds true. While the ΔH value can be chemically tuned about the substituent induction effects, the values of ΔS is difficult to predict because of manifold contributions in the solid state (*e.g.* solvent effect, degrees of freedom, free rotations, defects, vibrational contributions). It is also known that the ΔH value increases starting from monodenate (*e.g.* pyridine) over rigid bidentate (*bpy* – bipyridine, *pybzim* – 2-(2′-pyridyl)benzimidazole) to rigid tridentate ligands (*bzimpy* – 2,6-bis(benzimidazol-2-yl)pyridine or *bpp* – 2,6-bis(pyrazol-1-yl)pyridine) [12,13].

Herein we are reporting on two Fe(II) complexes coordinating either the ligand 2-(6-(pyrazol-1-yl)pyridin-2-yl)-1H-benzimidazole (**L_1H**) or the corresponding deprotonated base 2-(6-(pyrazol-1-yl)pyridin-2-yl)-1H-benzimidazolate (**L_1**), which are $[Fe(\mathbf{L_1H})_2](BF_4)_2$ and $[Fe(\mathbf{L_1})_2]$, hereafter **1** and **2**. The applied synthetic route is shown in Fig. 1. A similar synthetic route was described recently for a homoditopic ligand consisting of two L_1H subunits sharing the benzene moiety of the benzimidazole [14]. L_1H was prepared before in a different synthetic way and was applied coordinated to Ru(II) in the transfer hydrogenation of ketones [15,16].

2. Experimental

2.1. Chemicals and handling

All chemicals of reagent grade quality (including reactant ethyl 6-bromopyridine-2-carboxylate) were purchased and used as received. The solvents as dichloromethane and methanol used for the preparation of the complexes have been purified by distillation

* Corresponding authors at: Department of Chemistry, Faculty of Natural Sciences, University of SS Cyril and Methodius, 91701 Trnava, Slovakia (C. Rajnák, R. Boča). Institute of Nanotechnology, Karlsruhe Institute of Technology (KIT), 76021 Karlsruhe, Germany (M. Ruben).

E-mail addresses: cyril.rajnak@ucm.sk (C. Rajnák), mario.ruben@kit.de (M. Ruben), roman.boca@stuba.sk (R. Boča).

http://dx.doi.org/10.1016/j.poly.2017.06.035
0277-5387/

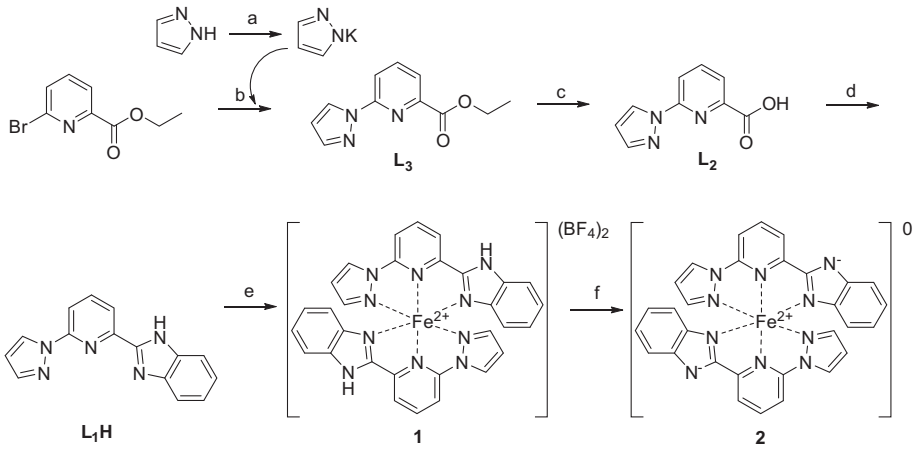

Fig. 1. Synthetic path: a) K, diglyme, Ar, 75 °C, overnight; b) 3 days, Ar, 110 °C; c) 2 M NaOH, EtOH, reflux, 2 h; d) *o*-phenylenediamine, polyphosphoric acid, reflux, 8 h, Ar; e) $Fe(BF_4)\cdot 6H_2O$, CH_2Cl_2/MeOH 1:2, 40 °C, Ar, overnight; f) CH_2Cl_2/MeOH 1:2, Na_2CO_3, 40 °C, Ar.

from suitable drying agents under inert argon atmosphere. Other solvents and liquid compounds: diethylenedimethylether (diglyme), HCl, water and polyphosphoric acid (PPA) were used as received.

CAUTION. Handling of alkaline earth metals e.g. K is potentially dangerous due to their flammable properties in the air. It should be handled with care in small quantities or in protecting atmosphere during their using.

2.2. Physical measurements

Elemental analysis was carried out by the analyzer vario MICRO cube (Analysensysteme Elementar) and Flash 2000 CHNS/O apparatus (Thermo Scientific). Melting points were studied by Buchi540 in narrow glass tubes or thermo-microscopically by Kofler hot-stage microscope at 4 °C·min^{-1} and reported without corrections. The solid KBr for FT-IR measurements was kept against absorption of moisture in an oven at 60 °C before every measurement. A blank spectrum was recorded by the reference clean KBr sample. FT-IR spectra were measured by the diluting of compounds in KBr powder, well mixed and pressed to pellets (Spectrum GX, Perkin Elmer). Absorption UV–Vis spectra were carried out by two-beam UV–Vis–NIR spectrophotometer (Cary 500 Scan) and the baselines were measured with pure solvents before. Electrospray ionization time of flight (ESI-TOF) mass spectrometry was acquired on a micrOTOF-Q II (Bruker) spectrometer in the positive mode of ion polarity. The samples were dissolved in suitable solvents and filled up into the glass can. The NMR spectra of organic compounds were measured in deuterated DMSO-d_6 using by FT-NMR Spectrometer (Avance III 500, Bruker) and analyzed by TOPSPIN 1.2 software. Other measurements are specifying in separate paragraphs in details.

2.3. Synthesis of 6-pyrazol-1-yl-pyridine-2-caboxylic acid ethyl ester (***L₃***)

Into a three necked 250 cm^3 round bottom flask charged with small K metal cubes (1.09 g, 27.93 mmol, 0.83 eq) in diglyme solvent (100 cm^3) the crystalline pyrazole (2.29 g, 33.64 mmol, 1 eq) was added and treated to a dispersion under argon at 75 °C. The mixture was intensively stirred overnight to obtain milky solution of pyrazolate salt [17]. Ethyl 6-bromopyridine-2-carboxylate (5.1 g, 22.17 mmol) was added and reaction was stirred 3-days under Ar atmosphere at 110 °C to obtain yellowish suspension. Solvent was removed by distillation under vacuum (slowly from 100 to 155 °C, 8 mbar) on membrane pump. Water (100 cm^3) was added into the crude product and the mixture was extracted with CH_2Cl_2 (3 times 100 cm^3). Organic layers were combined and dried over the $MgSO_4$; further purification was not necessary. Yield 2.45 g, 50.8%, yellowish oil-solid mixture. ^{1}H NMR (500 MHz, DMSO-d_6, 25 °C) δ (ppm) 8.71 (d, J = 2.5 Hz, 1H), 8.19 (dd, J = 1.25 Hz, 1H), 7.99–7.93 (m, 2H), 7.75 (d, J = 1 Hz, 1H), 6.49 (t, J = 2 Hz, 1H), 4.48 (q, J = 7.2 Hz, 2H), 1.46 (t, J = 7.25 Hz, 3H). ^{13}C NMR (500 MHz, DMSO-d_6, 25 °C) δ (ppm) 164.63, 151.44, 146.76, 142.47, 139.60, 127.63, 122.53, 115.92, 108.11, 61.97, 50.86, 14.28. ESI-TOF MS (CH_3CN): m/z = 240.191 (theoretical m/z = 240.210 [M]+Na$^+$).

2.4. Synthesis of 6-pyrazol-1-yl-pyridine-2-caboxylic acid (***L₂***)

A 50 cm^3 round bottom flask was charged with 6-pyrazol-1-yl-pyridine-2-caboxylic acid (2.45 g, 11.28 mmol), 12.32 cm^3 of 2 M NaOH (24.6 mmol, 2.18 eq) and 17 cm^3 of ethanol [18]. The reaction was heated up at reflux for 2 h and then it was allowed to cool down to room temperature. Rest of ethanol was removed by rotary evaporation. Water (5 cm^3) was added into crude yellowish mixture. The pH of the solution was adjusted to a value of 2.5 with 3 M HCl and 1 M HCl. The product precipitated as off-white solid. It was collected by filtration and dried on membrane pump. Further purification was not necessary. Yield 2.07 g, 97.2%. $C_9H_7N_3O$: calcd. C 57.14, H 3.73, N 22.21; found C 57.22, H 3.56, N 22.32. Melting point 191–193 °C. ^{1}H NMR (500 MHz, C_2D_6OS) δ (ppm) 8.77 (d, J = 2.55 Hz, 1H), 8.17–8.13 (m, 2H), 7.98 (dd, J = 1.5 Hz, 1H), 7.86 (d, J = 1.45 Hz, 1H), 6.61 (t, J = 2.1 Hz, 1H). ^{13}C NMR (125 MHz, C_2D_6OS) δ (ppm) 165.23, 150.46, 146.86, 142.64, 140.94, 127.53, 122.47, 115.41, 108.54. FT-IR (KBr) ν/cm^{-1} 2996, 2881, 2650, 2582, 1710(s), 1640, 1593(s), 1529(m), 1482(w), 1458(w), 1398(s), 1332, 1316, 1286(s), 1211(m), 1161, 1135, 1054, 1036, 993, 947(m), 835, 761(s), 724, 649 (w – weak, s – strong, m – medium). ESI-TOF MS (CH_3OH): m/z = 212.04 [M]+Na$^+$ (theoretical m/z = 212.04 [M]+Na$^+$).

2.5. Synthesis of 2-(6-pyrazol-1-yl-pyridin-2-yl)-1H-benzoimidazole (***L₁H***)

A 50 cm^3 flask was charged with *o*-phenylenediamine (0.94 g, 8.72 mmol), 6-pyrazol-1-yl-pyridine-2-caboxylic acid (1.5 g, 7.93 mmol) and 85% polyphosphoric acid (7.26 cm^3, 12.41 g, 107.65 mmol). The reaction was refluxed for 8 h under argon. Then it was allowed to cool down and carefully poured on a 400 cm^3 ice water. Blue precipitate was stirred for 1 h. Then Na_2CO_3 (sat.aq.)

was added until pH was adjusted to a value of 7 (pink color). The product was filtered, washed with water (20 cm^3) and then dried in an oven (60 °C). Yield: 1.8 g, 87%. Melting point 206–208 °C. $C_{15}H_{11}N_5$: calcd. C 68.95, H 4.24, N 26.80; found C 68.84, H 4.55, N 26.92. ^{1}H NMR (500 MHz, C_2D_6OS) δ (ppm) 13.07 (s, 1H), 9.24 (d, J = 2.5 Hz, 1H), 8.20 (d, J = 7.5 Hz; 1H), 8.14 (t, J = 7.75 Hz, 1H), 7.99 (d, J = 8 Hz, 1H), 7.88 (d, J = 1.5 Hz, 1H), 7.69 (s, 2H), 7.27 (s, 2H), 6.92 (t, J = 1.5 Hz, 1H). ^{13}C NMR (125 MHz, C_2D_6OS) δ (ppm) 150.42, 149.88, 146.96, 142.58, 140.84, 128.19, 118.68, 112.13, 108.20. UV–Vis (CH_2Cl_2/MeOH; 5:1): λ_{max} (ε, M^{-1} cm^{-1}) 321 (25755), 277 (5441), 262 (11729). FT-IR (KBr) ν/cm^{-1} 3121, 1967, 1927, 1887, 1850, 1775, 1667(w), 1603(m), 1577(s), 1518 (m), 1467(s), 1437(w), 1409(w), 1395(m), 1316(m), 1280, 1233, 1205, 1152, 1146, 1113, 1066(m), 1048, 1041, 1007, 992, 94(m), 828, 809, 779, 767, 747(s), 655, 558 (w – weak, s – strong, m – medium). ESI-TOF MS (CH_3OH): m/z = 545.16 (theoretical m/z = 545.19 $[M+Na^+]$).

2.6. Synthesis of $[Fe(\mathbf{L_1H})_2](BF_4)_2$(**1**)

In a 100 cm^3 two-necked round-bottomed flask the ligand $\mathbf{L_1H}$ (0.25 g, 0.96 mmol) was dissolved in methanol (25 cm^3) and dichloromethane (5 cm^3). The solution was degassed with argon for 30 min. and $Fe(BF_4)_2{\cdot}6H_2O$ (0.162, 0.48 mmol) was added once to the ligand solution. The mixture was stirred at 40 °C overnight with color changing to red. The suitable single crystals were obtained by controlled evaporation of solvents (**1b**). Another type of crystals with good quality was obtained also by recrystallization from CH_3CN (**1a**). Yield 0.202 g, 56.2%. Melting point 190–192 °C. $C_{30}H_{22}B_2F_8FeN_{10}$ (dried crystals without lattice bond solvent molecules): calcd. C 47.91, H 2.95, N 18.63; found C 47.70, H 3.07, N 18.58. ESI-TOF MS (MeOH/CH_2Cl_2): m/z = 289.05 (theoretical m/z = 289.06 $[M]^{2+}$); m/z = 665.09 (theoretical m/z = 665.14 $[M]^+$). FT-IR (KBr) ν/cm^{-1} 3382, 3122, 3066, 2924, 2854, 1734, 1607(m), 1574(m), 1523(m), 1504, 1473(s), 1440, 1405(m), 1375, 1349, 1324(m), 1278, 1232, 1206, 1178, 1053(BF_4), 992, 955, 940, 915, 835, 807, 750(s), 852, 597, 523, 455, 434. UV–Vis (CH_2Cl_2/MeOH; 5:1): λ_{max} (ε, M^{-1} cm^{-1}) = 321(53465), 277(8663), 262(20297). UV–Vis (Nujol) $\nu_{max}/10^3$ - cm^{-1} (relat. absorb.): 19.65(0.33), 23.15(0.34), 29.07(0.54).

2.7. Synthesis of $[Fe(\mathbf{L})_2]^0$ (**2**)

In a 100 cm^3 two-necked round-bottomed flask a crude non-crystalline solid complex **1** was dissolved in methanol (25 cm^3) and dichloromethane (5 cm^3) under argon atmosphere. After 30 min. of stirring a solid Na_2CO_3 (0.142 g, 1.34 mmol, 5 eq) was added and the mixture stirred at 40 °C overnight. Unreacted carbonate was removed by filtration. Dark red precipitate was obtained on the rotary evaporator. Yield 0.141 g, 91%. Melting point 176–178 °C. $C_{30}H_{22}B_2F_8FeN_{10}$: calcd. C 62.51, H 3.50, N 24.30; found C 62.68, H 3.37, N 24.23. ESI-TOF MS (MeOH/CH_2Cl_2): m/z = 577.09 (theoretical m/z = 577.13 $[M+H]^+$); m/z = 284.07 (theoretical m/z = 284.09 $[M+Na]^+$). FT-IR (KBr) ν/cm^{-1} 3396, 3106, 2971, 2921, 2856, 2679, 1189, 1797, 1713, 1602(s), 1576(s), 1522 (m), 1469(s), 1394(s), 1344, 1317, 1283, 1237, 1205(m), 1151, 1137, 1126, 1065(m), 1041(m), 1001, 992, 979, 938(m), 916, 855, 812(m), 766(m), 735, 718, 654, 623, 590, 534, 512, 463, 431, 409 (w – weak, s – strong, m – medium). UV–Vis (CH_2Cl_2/MeOH; 5:1): λ_{max} (ε, M^{-1} cm^{-1}) 321(38596), 277(2005), 262(9273). UV–Vis (Nujol) $\nu_{max}/10^3$ cm^{-1} (relat. absorb.): 15.02(0.08), 20.62 (0.34), 29.33(0.63), 30.58(0.64).

2.8. X-ray structure determination

Single crystal X-ray data of **1a** were collected on a STOE IPDS 2 T diffractometer with graphite monochromated Mo Kα radiation (λ = 0.71073 Å). Using Olex2 [19], the structure was solved with the SHELXS [20] structure solution program using Direct Methods and refined with the SHELXL [21] refinement package using Least Squares minimization. Refinement was performed with anisotropic temperature factors for all non-hydrogen atoms. The positions of the hydrogen atoms were calculated on idealized positions. The crystal data and the parameters of the structure refinement for $[Fe(L_{1H})_2](BF_4)_2{\cdot}2CH_3CN$ are listed in Table 1.

For **1b** the positions of lattice bond solvent molecules could not be refined properly. Therefore their contribution was subtracted from the electron density and a modified *hkl* file was calculated using the SQUEEZ algorithm provided by the program package PLATON [22]. Additionally, the solvent accessible void per unit cell was calculated (1760 Å^3). Assuming a molecular volume of 40 Å^3 for a methanol molecule there would be space for 44 solvent molecules in the unit cell resulting to an approximate composition of $[Fe(\mathbf{L_1H})_2](BF_4)_2{\cdot}5.5MeOH$ for **1b**.

2.9. Magnetic and photomagnetic experiments

Magnetic measurements were performed on SQUID magnetometers (MPMS-XL7 and MPMS-XL5, Quantum Design). For the standard magnetic measurement in the dark, the temperature dependent magnetization was recorded at B_{DC} = 0.1 T as an external magnetic field. The temperature sweeping rate was 1 K min^{-1} and it was the same for cooling and for heating modes. Gelatin capsules were used as sample holders in the temperature range 5 ↔ 400 K. In the case of high-temperature mode (300–600 K), a special heating setup was used and high temperature sample holder consisted of quartz-glass tube and Teflon filler. The diamagnetic corrections of the molar magnetic susceptibilities were applied using Pascal constants. For the photomagnetic experiments a small amount of sample (≈0.1 mg) was introduced onto a transparent tape and mounted into the sample holder. The exact weight of samples was obtained by weighting and also verified by compar-

Table 1
Crystal data for **1a** and **1b**.

	1a (**1**·2CH_3CN)	**1b** (**1** as solvent free)
Empirical formula	$C_{34}H_{28}B_2N_{12}F_8Fe$	$C_{30}H_{22}B_2N_{10}F_8Fe$
Formula weight (g mol^{-1})	834.15	752.04
T (K)	180	180
Crystal system	orthorhombic	monoclinic
Space group	*Pbca*	*C*2/*c*
Crystal size (mm)	0.42 × 0.39 × 0.12	0.12 × 0.04 × 0.03
Z	8	8
a (Å)	17.1559(7)	17.138(3)
b (Å)	19.1180(9)	18.447(4)
c (Å)	21.9202(7)	24.960(5)
β (°)		104.76(3)
V (Å^3)	7189.5(5)	7631(3)
Calculated density D_{calc} (g cm^{-3})	1.541	1.309
Absorption coefficient (mm^{-1})	0.507	0.469
Reflections collected	25504	18245
Independent reflections	6757 [R_{int} = 0.1317, R_σ = 0.0804]	7128 [R_{int} = 0.0950, R_σ = 0.1440]
Ind. reflections with $I \geq 2\sigma(I)$	4416	3026
Data/restraints/parameters	6757/0/525	7128/20/450
Goodness-of-fit (GOF) on F^2	0.983	0.860
Final R indices [$I \geq 2\sigma$ (I)]	R_1 = 0.0644, wR_2 = 0.1685	R_1 = 0.0693, wR_2 = 0.1730
R indices [all data]	R_1 = 0.0943, wR_2 = 0.1847	R_1 = 0.1556, wR_2 = 0.2061
Largest diff. peak/hole (e Å^{-3})	1.08/−0.56	0.60/−0.53
CCDC No	1497850	1038558

ison of thermal χT *versus* T curve with that of a more accurately weighed sample of the same compound. After the cooling to 10 K, the sample, now in the low spin state, was irradiated (637 nm or 532 nm) and the change in magnetization was followed. When the saturation point had been reached, the light was switched off, the temperature was increased at a rate 0.3 K min^{-1}, and the magnetization was measured at 1 K intervals. The value of T(LIESST) was determined from the minimum of the d(χT)/dT *versus* T curve for the thermally induced relaxation process.

3. Results and discussion

3.1. X-ray structure

The molecular structure of **1** is shown in Fig. 2 along with the packing in the crystal lattice for **1a**.

The structure is formed of mononuclear {FeN_6} complexes of quasi-octahedral shape. Inspection to metal-ligand distances (Table 2) confirms that the geometry assembles a compressed tetragonal bipyramid with the averaged equatorial distances Fe-N_{eq} = 1.90 and axial ones Fe-N_{ax} = 1.97 Å, typical for low-spin configuration of Fe(II). The cationic units are placed in the solid state in the way that the benzene rings of the benzimidazole moieties show a π-π stacking at the distances of ring centroids about 3.52 Å.

3.2. Magnetic data

The temperature dependence of the effective magnetic moment for **1** is plotted in Fig. 3a. This is split into two overlapping segments according to the hardware setup ("normal" *versus* "oven"). The low-temperature part is far from the pure $S = 0$ behavior since μ_{eff} = 2.40–2.45 μ_B in the temperature range 25–135 K. One can explain this either by few paramagnetic impurities such as Fe(III) admixture, or by some frozen portion of high-spin Fe(II). Above 135 K the effective magnetic moment starts to increase and reaches a saturation of μ_{eff} = 5.00 μ_B at T = 580 K. This is due to the complete spin transition to $S = 2$ state.

Fig. 3b shows the temperature dependence of the effective magnetic moment for **2**. Between 50 and 150 K it stays almost constant at μ_{eff} = 2.4 μ_B whereas below 50 K it drops down to μ_{eff} = 1.4 μ_B. Above 150 K the effective magnetic moment slightly increases and above 300 K it grows more rapidly until μ_{eff} = 3.7 μ_B at T = 390 K. Such an increase may be seen as the on-set of the spin crossover.

Table 2
Bond lengths (Å) and bond angles (°) of **1a** at 180 K.

Fe(1)–N(3)	1.901(3)	N(3)–Fe(1)–N(8)	178.95(12)
Fe(1)–N(8)	1.898(3)	N(3)–Fe(1)–N(6)	99.79(11)
Fe(1)–N(6)	1.966(3)	N(8)–Fe(1)–N(6)	80.10(11)
Fe(1)–N(1)	1.959(3)	N(3)–Fe(1)–N(1)	80.00(11)
Fe(1)–N(4)	1.981(3)	N(8)–Fe(1)–N(1)	101.04(11)
Fe(1)–N(9)	1.982(3)	N(6)–Fe(1)–N(1)	90.42(12)
		N(3)–Fe(1)–N(4)	80.79(11)
		N(8)–Fe(1)–N(4)	98.17(11)
		N(6)–Fe(1)–N(4)	92.91(12)
		N(1)–Fe(1)–N(4)	160.79(11)
		N(3)–Fe(1)–N(9)	99.49(11)
		N(8)–Fe(1)–N(9)	80.62(11)
		N(6)–Fe(1)–N(9)	160.72(11)
		N(1)–Fe(1)–N(9)	93.21(11)
		N(4)–Fe(1)–N(9)	89.86(12)

The DC magnetic data was analyzed in terms of the Ising-like model that is equivalent to the regular solution model of the spin crossover [23–25]. The pure spin state ($S = 2$ and/or $S = 5/2$) were described by the Curie–Weiss law in the form

$$\chi_S = (N_A \mu_0 \mu_B^2 / k_B) g_S^2 S(S+1)/[3(T - \Theta_S)] + \alpha_S \quad (1)$$

where the physical constants adopt their usual meaning. The Weiss constant Θ_S recovers either the intermolecular interactions for $S = 5/2$, or the zero-field splitting for $S = 2$. The $S = 0$ state is magnetically silent ($g = 0$) but some temperature-independent paramagnetism α_{LS} can be in the play since there are low-lying excited states belonging to the HS state.

The spin crossover is characterized by the temperature development of the high-spin mole fraction $x_{HS} = f(T)$. This quantity enters an implicit equation to be solved by an iterative procedure

$$x_{HS} = (1 - x_{PI})F/(F+1) \quad (2)$$

with the factor

$$F = r_{eff} \exp\{-[\Delta_{eff} - 2\gamma(2x_{HS} - 1)]/k_B T\} \quad (3)$$

Here Δ_{eff} that is an energy gap proportional to the enthalpy of the spin transition $\Delta H = R\Delta_{eff}$; r_{eff} is an effective degeneracy ratio of the spin states $r_{eff} \gg (2S_{HS} + 1)/(2S_{LS} + 1)$ owing to the vibrational degrees of freedom and it is proportional to the entropy of the transition $\Delta S = R(\ln r_{eff})$; γ stands for the eventual solid-state cooperativeness. The value of r_{eff} is either a free parameter, or a quantity evaluated from averaged vibrational modes of 15 vibrations of the chromophore

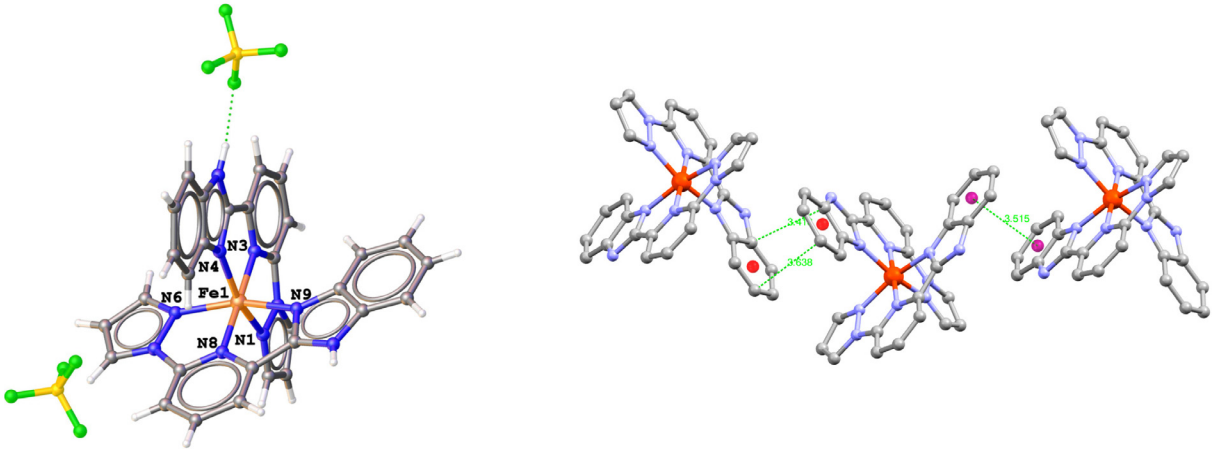

Fig. 2. Molecular structure of **1a** and the π-π stacking in the crystal lattice. (Hydrogen atoms omitted for clarity.)

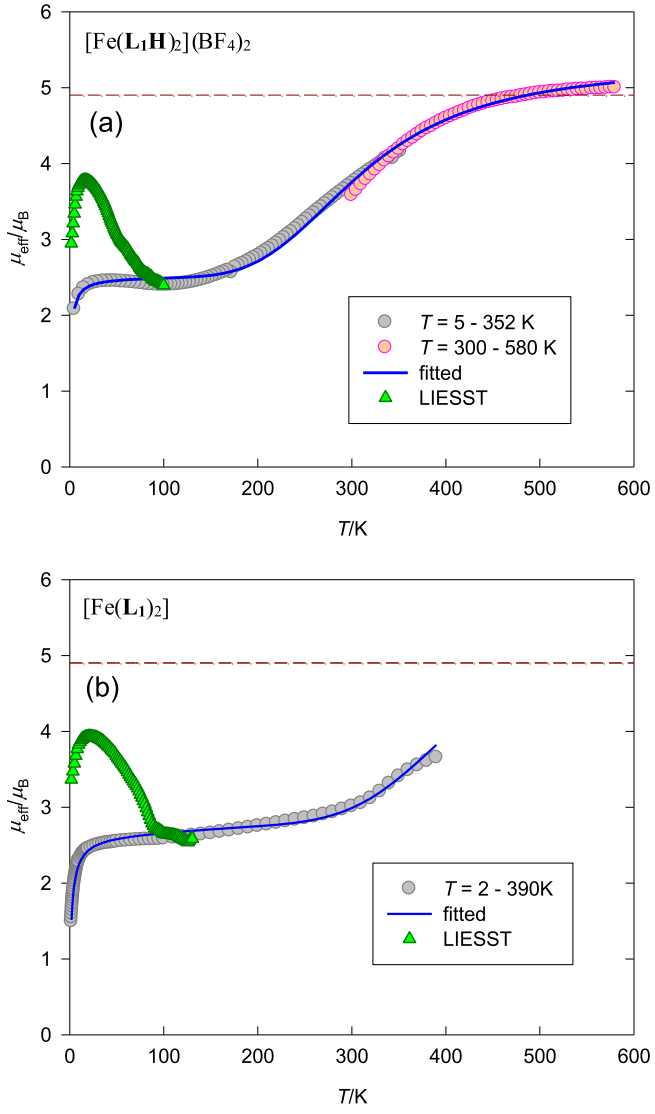

Fig. 3. Temperature evolution of the effective magnetic moment for **1** and **2**. Line – fitted data. Dashed horizontal line represents spin-only value for high-spin Fe(II).

$$r_{\mathrm{eff}} = \frac{2S_{\mathrm{HS}}+1}{2S_{\mathrm{LS}}+1}\cdot\left[\frac{1-\exp(h\bar{\nu}_{\mathrm{LS}}/k_{\mathrm{B}}T)}{1-\exp(h\bar{\nu}_{\mathrm{HS}}/k_{\mathrm{B}}T)}\right]^{15} \quad (4)$$

The balance for the molar susceptibility is then

$$\chi_{\mathrm{mol}} = x_{\mathrm{PI}}\cdot\chi_{S=5/2} + x'_{\mathrm{HS}}\cdot\chi_{S=2} + (1-x'_{\mathrm{HS}}-x_{\mathrm{PI}})\cdot\chi_{S=0},$$
$$x'_{\mathrm{HS}} = x_{\mathrm{HS}}(1-x_{\mathrm{PI}}) \quad (5)$$

for the model A, and

$$\chi_{\mathrm{mol}} = x_{\mathrm{fr}}\cdot\chi_{S=2} + x'_{\mathrm{HS}}\cdot\chi_{S=2} + (1-x'_{\mathrm{HS}}-x_{\mathrm{fr}})\cdot\chi_{S=0},$$
$$x'_{\mathrm{HS}} = x_{\mathrm{HS}}(1-x_{\mathrm{fr}}) \quad (6)$$

for the model B. With these formulae, always $x'_{\mathrm{HS}} < 1$ holds true.

During the fitting procedure it was observed that for $\gamma \sim 0$ (which is the case of **1** and **2**), the free parameters r_{eff} and Δ_{eff} become mutually strongly correlated: with increasing Δ_{eff} also r_{eff} increases while the ratio $T_c = \Delta H/\Delta S$ stays almost constant. Therefore an advanced model with vibrations *via* Eq. (4) has been utilized hereafter. A fitting procedure converged to the set of magnetic and spin crossover parameters as listed in Table 3. The fitted data is shown as lines in Fig. 3. One can conclude that the fit is good as the discrepancy factor R is low. The results of the model B is essentially the same with a different interpretation of the low-temperature tail.

Table 3
Magnetic and spin crossover parameters for **1** and **2**.

Parameter	**1**, model A	**2**, model A
$\alpha_{\mathrm{LS}}/10^{-9}$ m^3 mol^{-1}	1.0	6.9(14)
g_{HS}	2.13(4)	2.24
g_{PI}	[2.0]	[2.0]
Θ_{PI}/K	−2.2(7)	−3.9(2)
x_{PI}	0.179(8)	0.199(3)
γ	~0	~0
$\Delta_{\mathrm{eff}}/k_{\mathrm{B}}$ /K	1119(236)	2188(392)
$\bar{\nu}_{\mathrm{LS}}$/cm^{-1}	455	431(264)
$\bar{\nu}_{\mathrm{LS}}/\bar{\nu}_{\mathrm{HS}}$	1.24(8)	[1.4]
R-factor	0.017	0.027
Reconstructed		
ΔH/kJ mol^{-1}	9.30	18.2
ΔS/J K^{-1} mol^{-1} at $x_{\mathrm{LS}} = x_{\mathrm{HS}}$	27.1	40.5
$(\Delta H/\Delta S)$/K at $x_{\mathrm{LS}} = x_{\mathrm{HS}}$	343	449

The above mentioned thermally induced SCO properties of both compounds are unlike to the typical spin crossover between the low-spin state ($S = 0$) and the high-spin state ($S = 2$). An incompleteness of the spin crossover at $T = 390$ K can be explained by a rather high critical temperature $T_c > 390$ K. Understanding of a low-temperature residue at $\mu_{\mathrm{eff}}/\mu_{\mathrm{B}}$ is trickier. The model A assumes that there is a paramagnetic impurity x_{PI} of the high-spin Fe(III) centers ($S = 5/2$, $g_{\mathrm{PI}} = 2$) and some intermolecular interactions are responsible for the drop of the effective magnetic moment. The model B assumes that a portion x_{fr} of the high-spin states ($S = 2$) remains frozen and does not undergo the spin transition. The sizable drop of the effective magnetic moment is then caused by the zero-field splitting of the frozen HS molecules.

The reconstructed thermodynamic quantities for **2** are $\Delta H = 18.2$ kJ mol^{-1}, $\Delta S = 40.5$ J K^{-1} mol^{-1} (at $x_{\mathrm{LS}} = x_{\mathrm{HS}}$) and their ratio yields $T_c = \Delta H/\Delta S = 449$ K. All parameters seem be realistic except the Weiss constant Θ_{PI} that is too negative in order to be ascribed to the (weak) intermolecular interactions. For the model B the reconstructed thermodynamic quantities are essentially the same but the negative Weiss constants is interpreted as a consequence of the zero-field splitting for $S = 2$ Fe(II) centers.

Thermodynamic parameters for the neutral Fe(II) spin crossover systems are listed in Table 4 for comparison. It can be seen that according to ΔH the systems fall into three groups according to the denticity of the ligands. Typically, $\Delta H = 7$–18 kJ mol^{-1} and $\Delta S = 38$–60 J K^{-1} mol^{-1} for systems with $T_c = 170$–425 K, as results from DSC data and analysis of magnetic data. The complex under study occupies the higher edge of the series owing to rather high enthalpy of the spin transition.

The LIESST effect was investigated by irradiation of samples with green (532 nm) and/or red (637 nm) laser and we found that later wavelength was much more effective for both compounds. After the irradiation, magnetic properties of samples were monitored in the dark (Fig. 3, green triangles). On heating, the increase of the effective magnetic moment is attributed to zero field splitting effect of metastable high-spin Fe(II) species. Around 20 K, both compounds reach the maximum at 4.0 μ_{B} (compound **1**) and 3.8 μ_{B} (compound **2**) which corresponds to 56% and 64% of metastable high-spin Fe(II), respectively. With further heating, the thermally induced gradual high-spin → low-spin relaxation takes the place and the first derivative of the product function d(χT)/dT *versus* T allowed determining T(LIESST) temperatures at 41 K and 81 K, respectively. This is quite surprising dispersion of T(LIESST) parameters of two compounds with such similar structural and thermally induced SCO properties. However detailed look on d(χT)/dT *versus* T curve of **1** revealed at least another three relaxation processes at

Table 4
Comparison of the thermodynamic parameters for neutral spin crossover systems.

Selected systems	Method [a]	T_c [K] [b]	ΔH [kJ mol^{-1}]	ΔS [J K^{-1} mol^{-1}]	$\Delta H/\Delta S$ [K]	γ/k_B [K]	Ref.
[Fe(*py*)$_2$(*phen*)(NCS)$_2$]·0.5py	DSC	106	3.7	37.0	100		[26]
[Fe(*py*)$_2$(*bpym*)(NCS)$_2$]·0.5py	DSC	116	6.5	56	116		[26]
[Fe(*btr*)$_2$(NCS)$_2$]·H$_2$O	DSC	132	10.2	76.4	134		[27]
	MgX	141	2.62	18.5	142	112	[12]
[Fe(5NO$_2$-sal(1,4,7,10))]	MgX	145(↑)	7.6	50	152	280	[28]
		180(↑)					
Bidentate ligands							
[Fe(*phen*)$_2$(NCS)$_2$]	Cal	176.3	8.60	48.8	176		[29]
α-[Fe(*dppa*)$_2$(NCS)$_2$]	MgX	178	6.9	39	177	160	[30]
[Fe(*dpyatriz*)$_2$(SCN)$_2$]	DSC	200	7.45	37.7	198		[31]
[Fe(*bpy*)$_2$(NCS)$_2$]	DSC	212	10	48	208		[32]
[Fe(PM-BiA)$_2$(NCS)$_2$]	DSC	168	10.06	59.9	168		[33]
		173	10.05	58.1	173		
[Fe(*phen*)$_2$(NCSe)$_2$]	Cal	231.3	11.6	51.2	227		[33]
Tridentate ligands							
[Fe(*bzimpy*$_{-1H}$)$_2$·H$_2$O	MgX-pi	424(↑)	18.1	43	421	519	[34]
	DSC	425(↑)					[35]
[Fe(*pzpybzim*$_{-1H}$)$_2$]	MgX-pi		18.2	40.5	449		This work

[a] Cal – adiabatic calorimetry; DSC – differential scanning calorimetry; MgX – fitting the magnetic susceptibility (Ising-like model). MgX-pi – model with a paramagnetic impurity. Warning: calculated data might be model-dependent.
[b] T_c – critical temperature for $x_{HS} = x_{LS}$; peak values T_p are reported for DSC and adiabatic calorimetry.

63 K, 73 K and 87 K (see Supporting Information) which indicates complicated thermal relaxation of the photoexcited high-spin state of **1**.

4. Conclusions

In conclusion, the pyrazol-benzimidazol-pyridine ligand acts analogously as the 2,6-bis(benzimidazol-2-yl)pyridine one and facilitates the spin crossover between $S = 0$ and $S = 2$ spin states of the Fe(II) centers in both, the ionic and charge-neutral complexes [Fe(*pzpybzim*)$_2$](BF$_4$)$_2$ and [Fe(*pzpybzim*$_{-1H}$)$_2$], respectively. The critical temperature in both cases lies above the room temperature (T_c = 343 and 449 K). Both compounds exhibit the LIESST effect with T(LIESST) temperatures of 41 K and 81 K, respectively.

Acknowledgments

Slovak grant agencies (VEGA 1/0522/14, VEGA 1/0919/17, APVV-14-0078, APVV 16-0039), COST Action CM1305 (ECOSTBio), STU Grant scheme for Support of Excellent Teams of Young Researchers and the Marie Curie RTN project No. PITN-GA-2009-238804, are acknowledged for the financial support. We thank the KIT-INT staff for their technical support.

Appendix A. Supplementary data

CCDC 1497850 and 1038558 contains the supplementary crystallographic data for **1a** and **1b**. These data can be obtained free of charge via http://www.ccdc.cam.ac.uk/conts/retrieving.html, or from the Cambridge Crystallographic Data Centre, 12 Union Road, Cambridge CB2 1EZ, UK; fax: (+44) 1223-336-033; or e-mail: deposit@ccdc.cam.ac.uk. Supplementary data associated with this article can be found, in the online version, at http://dx.doi.org/10.1016/j.poly.2017.06.035.

References

[1] P. Gütlich, H.A. Goodwin, Spin Crossover in Transition Metal Compounds I, Springer, Berlin, 2004.
[2] M.A. Halcrow, Coord. Chem. Rew. 253 (2009) 2493.
[3] L.J. Kershaw Cook, R. Mohammed, G. Sherborne, T.D. Roberts, S. Alvarez, M.A. Halcrow, Coord. Chem. Rew. 289–290 (2015) 2.
[4] I. Šalitroš, O. Fuhr, M. Ruben, Materials 7 (2016) 585.
[5] I. Šalitroš, L. Pogány, M. Ruben, R. Boča, W. Linert, Dalton Trans. 43 (2014) 16584.
[6] D. Gentili, F. Liscio, N. Demitri, B. Schäfer, F. Borgatti, P. Torelli, B. Gobaut, G. Panaccione, G. Rossi, A. Degli Esposti, M. Gazzano, S. Milita, I. Bergenti, G. Ruani, I. Šalitroš, M. Ruben, M. Cavallini, Dalton Trans. 45 (2016) 134.
[7] R. Boča, P. Baran, L. Dlháň, H. Fuess, W. Haase, F. Renz, W. Linert, I. Svoboda, R. Werner, Inorg. Chim. Acta 260 (1997) 129.
[8] R. Boča, P. Baran, M. Boča, L. Dlháň, H. Fuess, W. Haase, W. Linert, B. Papánková, R. Werner, Inorg. Chim. Acta 278 (1998) 190.
[9] I. Šalitroš, N.T. Madhu, R. Boča, J. Pavlik, M. Ruben, Monatsh. Chem. 140 (2009) 695.
[10] B. Schafer, C. Rajnák, I. Šalitroš, O. Fuhr, D. Klar, C. Schmitz-Antoniak, E. Weschke, H. Wende, M. Ruben, Chem. Commun. 40 (2013) 10986.
[11] K. Senthil Kumar, I. Šalitroš, B. Heinrich, O. Fuhr, M. Ruben, J. Mater. Chem. C 3 (2015) 1163.
[12] R. Boča, M. Boča, H. Ehrenberg, H. Fuess, W. Linert, F. Renz, I. Svoboda, Chem. Phys. 293 (2003) 375.
[13] R. Boča, M. Boča, Ľ. Dlháň, K. Falk, H. Fuess, W. Haase, R. Jaroščiak, B. Papánková, F. Renz, M. Vrbová, R. Werner, Inorg. Chem. 40 (2001) 3025.
[14] B. Schäfer, J.-F. Greisch, I. Faus, T. Bodenstein, I. Šalitroš, O. Fuhr, K. Fink, V. Schünemann, M.M. Kappes, M. Ruben, Angew. Chem. Int. Ed. 55 (2016) 10881.
[15] F. Zeng, Z. Yu, Organometallics 28 (2009) 1855.
[16] W. Luo, A. Li, S. Liu, H. Ye, Z. Li, Organometallics 35 (2016) 3045.
[17] D.L. Jameson, K.A. Goldsby, J. Org. Chem. 55 (1990) 4992.
[18] V. Theodorou, K. Skobridis, A.G. Tzakos, V. Ragoussis, Tetrahedron Lett. 48 (2007) 8230.
[19] O.V. Dolomanov, L.J. Bourhis, R.J. Gildea, J.A.K. Howard, H. Puschmann, J. Appl. Cryst. 42 (2009) 339.
[20] G.M. Sheldrick, Acta Cryst. A64 (2008) 112.
[21] G.M. Sheldrick, Acta Cryst. C71 (2015) 3.
[22] A.L. Spek, J. Appl. Cryst. 36 (2003) 7;
A.L. Spek, Acta Cryst. D65 (2009) 148.
[23] R. Boča, Theoretical Foundations of Molecular Magnetism, Elsevier, Amsterdam, 1999.
[24] R. Boča, A Handbook of Magnetochemical Formulae, Elsevier, Amsterdam, 2012.
[25] R. Boča, W. Linert, Monatsh. Chem. 134 (2003) 199.
[26] R. Claude, J.A. Real, J. Zarembowitch, O. Kahn, L. Ouahab, D. Grandjean, K. Boukheddaden, F. Varret, A. Dworkin, Inorg. Chem. 29 (1990) 4442.
[27] J.P. Martin, J. Zarembowitch, A. Dworkin, J.G. Haasnoot, E. Codjovi, Inorg. Chem. 33 (1994) 2617.
[28] V. Petrouleas, J.-P. Tuchagues, Chem. Phys. Lett. 137 (1) (1987) 21.
[29] M. Sorai, S. Seki, J. Phys. Chem. Solids 35 (1974) 555.
[30] G.S. Matouzenko, A. Bousseksou, S. Lecocq, P.J. van Koningsbruggen, M. Perrin, O. Kahn, A. Collet, Inorg. Chem. 36 (1997) 5869.
[31] M. Quesada, M. Monrabal, G. Aromi, V.A. de la Pena, M. O'Shea, E. Gich, O. Molins, S.J. Roubeau, E.J. Teat, P.Gamez MacLean, J. Reedijk, J. Mater. Chem. 6 (2006) 2669.
[32] S.K. Kulshreshtha, R.M. Iyer, Chem. Phys. Lett. 108 (1984) 501.
[33] J.-F. Letard, P. Guionneau, L. Rabardel, J.A.K. Howard, A. Goeta, D. Chasseau, O. Kahn, Inorg. Chem. 37 (1998) 4432.
[34] R. Boča, F. Renz, M. Boča, H. Fuess, W. Haase, G. Kickelbick, W. Linert, M. Vrbova-Schikora, Inorg, Chem. Comm. 8 (2005) 227.
[35] B. Papánková, M. Vrbová, R. Boča, P. Šimon, K. Falk, G. Miehe, H. Fuess, J. Thermal Anal. 67 (2002) 72.